Available online at www.sciencedirect.com

ScienceDirect

Advances in Space Research 55 (2015) 2149–2165

ADVANCES IN SPACE RESEARCH (a COSPAR publication)

www.elsevier.com/locate/asr

Radio reflection imaging of asteroid and comet interiors I: Acquisition and imaging theory

Paul Sava [a,*], Detchai Ittharat [a], Robert Grimm [b], David Stillman [b]

[a] Center for Wave Phenomena, Colorado School of Mines, 1500 Illinois Street, Golden, CO 80401, USA
[b] Planetary Science Directorate, Southwest Research Institute, 1050 Walnut St. #300, Boulder, CO 80302, USA

Received 3 February 2014; received in revised form 15 October 2014; accepted 15 October 2014
Available online 18 November 2014

Abstract

Imaging the interior structure of comets and asteroids can provide insight into their formation in the early Solar System, and can aid in their exploration and hazard mitigation. Accurate imaging can be accomplished using broadband wavefield data penetrating deep inside the object under investigation. This can be done in principle using seismic systems (which is difficult since it requires contact with the studied object), or using radar systems (which is easier since it can be conducted from orbit). We advocate the use of radar systems based on instruments similar to the ones currently deployed in space, e.g. the CONSERT experiment of the Rosetta mission, but perform imaging using data reflected from internal interfaces, instead of data transmitted through the imaging object. Our core methodology is wavefield extrapolation using time-domain finite differences, a technique often referred to as reverse-time migration and proven to be effective in high-quality imaging of complex geologic structures. The novelty of our approach consists in the use of dual orbiters around the studied object, instead of an orbiter and a lander. Dual orbiter systems can provide multi-offset data that illuminate the target object from many different illumination angles. Multi-offset data improve image quality (a) by avoiding illumination shadows, (b) by attenuating coherent noise (image artifacts) caused by wavefield multi-pathing, and (c) by providing information necessary to infer the model parameters needed to simulate wavefields inside the imaging target. The images obtained using multi-offset are robust with respect to instrument noise comparable in strength with the reflected signal. Dual-orbiter acquisition leads to improved image quality which is directly dependent on the aperture between the transmitter and receiver antennas. We illustrate the proposed methodology using a complex model based on a scaled version of asteroid 433 Eros.
© 2014 COSPAR. Published by Elsevier Ltd. All rights reserved.

Keywords: Wavefield imaging; Radar; Orbiters; Near-earth objects; Asteroids; Comets

1. Introduction

Asteroids and comets hold numerous clues for understanding the early evolution of the Solar System (Bottke et al., 2002; Festou et al., 2004). Asteroid and comet interiors are of great interest because they can provide information about the dynamical history of the object, related for example to accretion and differentiation, disruption and reassembly, metamorphism, etc. Near-Earth Objects (NEOs) are particularly interesting targets of investigation, not only because they pose hazards to Earth (Chapman, 2004), and also because they are accessible to human exploration, e.g. the Asteroid Retrieval Mission Brophy et al., 2012.

Different methods could be employed to study such small bodies, for example gravity and gradiometry (Hilton, 2002), magnetometry, and electromagnetic (EM) induction (Grimm, 2009). However, all such methods suffer from relatively low spatial resolution, a limitation that can

* Corresponding author.
E-mail address: psava@mines.edu (P. Sava).

http://dx.doi.org/10.1016/j.asr.2014.10.021
0273-1177/© 2014 COSPAR. Published by Elsevier Ltd. All rights reserved.

be addressed using wavefield techniques based on seismic or electromagnetic wave propagation, e.g. Ground Penetrating Radar (GPR). Asteroids and comets are regarded as objects with complex interior structure, which can be best revealed with methods exploiting accurate wave propagation. Wavefield techniques, for example, are successful at imaging complex imaging targets, as demonstrated numerous times in Earth applications, e.g. in exploration or global seismology, or for georadar near-surface investigation. Although highly effective, seismic methods are limited in the investigation of small NEOs due to their need for sensors (both sources and receivers) deployed directly on the studied object (Huebner and Greenberg, 2001; Walker et al., 2006; Roark et al., 2010). In contrast, georadar methods can operate using remote sensors that beam electromagnetic signals through empty space. Therefore, radar techniques appear to be a much simpler and more effective approach to the study of asteroids and comets, which is why we advocate this approach in our paper.

Space-based radio imaging has been proposed in the past (Safaeinili et al., 2002; Asphaug et al., 2004; Kofman and Safaeinili, 2004; Barucci et al., 2005; Asphaug et al., 2010), and the Rosetta Comet Nucleus Sounding Experiment by Radiowave Transmission (CONSERT) (Kofman et al., 2007) is an experiment designed to image the internal structure of comet 67P/Churyumov–Gerasimenko using radar signals emitted from an orbiter. We can distinguish two types of radar experiments based on transmission (electromagnetic waves propagate through the object and are recorded after crossing all internal interfaces), or on reflection (waves propagate inside the object and return toward the source after bouncing off the internal interfaces). This conceptual separation mimics conventional approaches used in Earth-based exploration seismology, i.e. cross-well tomography (based on transmission) and surface imaging (based on reflection) (Sherriff and Geldart, 2010). CONSERT is designed as a transmission tomography experiment based on sources activated at multiple positions from a moving orbiter and a single receiver on a lander anchored on the surface of the comet (Kofman et al., 2007). This experiment assumes that the dielectric properties of the comet allow electromagnetic waves to propagate all the way through (approximately 4 km) (Kofman and Safaeinili, 2004), which should allow tomography to characterize its internal structure. However, since this experiment is based on a single receiver, its angular coverage is likely to be limited, thus leading to relatively low resolution particularly in the main propagation direction. Resolution might be improved by using multiple internal scattering (Barriot et al., 1999; Benna et al., 2004), although this assumes that the signal remains strong enough after much longer propagation inside the comet and after undergoing reflection several times at considerable loss of energy.

We explore in this paper an alternative approach based on reflection imaging, instead of transmission imaging, and with multiple asynchronous orbiters, instead of one orbiter and a fixed lander. Reflection and transmission imaging are complementary to one-another, as they concentrate on different characteristics of the studied object. Transmission imaging can provide quick access to information about the propagation speed, for example by employing traveltime tomography for the propagation speed of electromagnetic waves (Kofman et al., 2007). However, this methodology has limited resolution with respect to interior interfaces between regions characterized by large contrasts of material properties. Reflection imaging, on the other hand, can achieve higher resolution, in particular when the transmission angular diversity is limited. Furthermore, reflection angular diversity can be increased using multiple (for example two) orbiters that revolve around the target object on different trajectories, and thus at different angular speeds. We demonstrate that reflection imaging with multiple orbiters is superior to imaging with a single orbiter due to the broader illumination resulting from combinations of transmitters and receivers at different positions relative to one-another. Moreover, multi-offset imaging has the ability to attenuate coherent noise common for single-offset imaging in complex media causing wavefield multi-pathing.

In the following, we proceed by summarizing wavefield reflection imaging for single or dual orbiters and then illustrate our method with a binary stochastic model of an asteroid interior. We focus primarily on describing radar acquisition in different configurations and on wavefield imaging techniques that can take advantage of broadband data to delineate accurately interior interfaces. Our methodology expands on earlier studies Benna et al., 2002; Carley and Heggy, 2008 investigating the applicability of radar wave propagation through complex comet nuclei using time-domain finite-difference wave propagation (FDTD). A companion paper, Grimm et al., 2014, addresses issues related to acquisition and target parameters and gives quantitative measures of image reconstruction accuracy; this paper also discusses some assumptions related to model parameters characterizing electromagnetic wave propagation speed and attenuation.

2. Imaging

Accurate imaging in inhomogeneous bodies requires reconstruction of wavefields inside the object under investigation from data recorded outside the object. Such wavefield-based imaging techniques have been developed primarily in the context of seismic exploration (Berkhout, 1982; Clærbout, 1985), but can be applied with minor modifications to the problem of imaging with electromagnetic waves, as well (Reynolds, 2011; Miller et al., 2010). We are considering, in particular, waves that can be generated from space-based radar systems similar to existing instruments, e.g. the Mars Advanced Radar for Subsurface and Ionosphere Sounding (MARSIS, $1-5$ MHz) (Picardi et al., 2004) or the Mars Shallow Subsurface Radar (SHARAD, 20 MHz) (Seu et al., 2007). For all numeric examples discussed in this paper, we use a Ricker wavelet (Ricker,

1944; Ricker, 1953) with a center frequency of 10 MHz, which fits in the range of the mentioned instruments. We assume that such radar systems can transmit and record broadband waveforms, thus allowing us to use wavefield imaging methodology.

As indicated earlier, we can generally consider two classes of experiments: reflection experiments constructed with transmitters and receivers on the same side of the object under investigation, and transmission experiments with transmitters and receivers on opposite sides. We concentrate here on reflection experiments. In this case, wavefield imaging methods consist of two main steps: wavefield reconstruction, i.e. a process which has the goal of building wavefields inside the object under investigation, and an imaging condition, i.e. a process which extracts information about the discontinuities inside the object from the reconstructed wavefields (Berkhout, 1982; Clærbout, 1985).

Wavefield reconstruction from recorded data requires knowledge of the relations governing wave propagation in the studied object, i.e. a wave-equation. In this paper, our focus is on the imaging aspects (i.e. acquisition style, data density, imaging procedure, etc.), therefore we assumed simplifications of the physics controlling in wave propagation. We assume, for example, that we can use a scalar wave equation (Aki and Richards, 2002)

$$\mathbf{L}(v)[W] = \frac{1}{v^2}\frac{\partial^2 W}{\partial t^2} - \nabla^2 W = f(\mathbf{x},t) \tag{1}$$

to describe the propagation and scattering occurring in an asteroid or a comet. The acoustic assumption allows for faster computing relative to a more accurate vector wave equation, although it ignores second order physical effects, for example attenuation in the medium or polarization changes during propagation. In Eq. 1, $\mathbf{L}$ is a wave operator which depends on the wave speed in the medium $v(\mathbf{x})$, and $W(\mathbf{x},t)$ represents the wavefield which is a four-dimensional function of space $\mathbf{x} = \{x,y,z\}$ and time t. In this framework, the velocity v depends primarily on the dielectric properties of the medium, and the wavefield W stands for one component of the electrical field, for example. The source function $f(\mathbf{x},t)$ also depends on position in space and time, although it is normally restricted to the position of the transmitters or receivers. Further generalizations of this equations are possible, for example scalar wave equations that account for the dielectric medium parameters, permeability $\mu(\mathbf{x})$ and permittivity $\epsilon(\mathbf{x})$, as well as attenuation, controlled by the medium conductivity $\sigma(\mathbf{x})$:

$$\mathbf{L}(\mu,\epsilon,\sigma)[W] = \mu\epsilon\frac{\partial^2 W}{\partial t^2} + \mu\sigma\frac{\partial W}{\partial t} - \nabla^2 W = f(\mathbf{x},t). \tag{2}$$

This equation implies that the attenuation is spatially variable, but does not change as a function of frequency. To first order, this is a reasonable assumption to model medium attenuation in typical asteroid rocks. However, since our focus in this paper is on acquisition and imaging, we do not discuss in greater details the impact of attenuation on the reconstructed images. The impact of attenuation in radar imaging is discussed by Grimm et al. (2014). In the following examples, we employ wave operator shown in Eq. 1.

From the data redundancy perspective, we can distinguish two main types of experiments: one in which sources and receivers are coincident, known as *zero-offset experiments*, and another in which sources and receivers are separated in space, known as *multi-offset experiments*. The imaging procedures used for both experiments share the need to reconstruct wavefields in the entire space under investigation and at all times, but differ in the way in which these wavefields are used to construct an image of the material discontinuities. In the following subsections, we provide a brief overview of wavefield imaging for each setup. Aside from the previously defined *wavefield* $W(\mathbf{x},t)$, the other two main objects relevant for this discussion are the *data* $D(\mathbf{r},t)$, representing the wavefield at all times restricted in space to the receiver coordinates ($\mathbf{r}$) and the *image* $R(\mathbf{x})$ of the interior of the object, representing the distribution of reflectors as a function of space ($\mathbf{x}$).

2.1. Zero-offset experiments

Imaging with zero-offset experiments is based on the exploding reflector model (Clærbout, 1985). A key assumption for this setup is that waves propagate along identical paths from a source to the reflectors and back to a receiver co-located with the source. Under this assumption, the propagation times along the two paths are identical, therefore, we can recast a zero-offset experiment as one in which the reflectors themselves act as sources triggered at time $t = 0$, but in which waves propagate at half the speed, Fig. 1.

The image is, thus, just the wavefield at time zero, so imaging simply reduces to the problem of reconstructing the wavefield at every location in space from the recorded data using time-reversal,

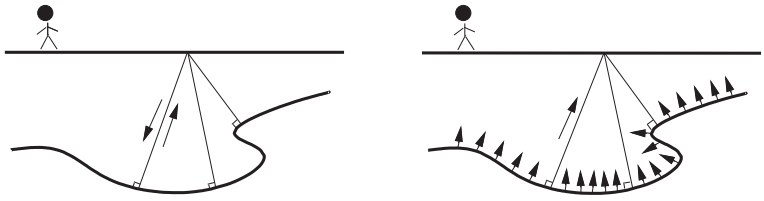
$$\mathbf{L}(v)[W(\mathbf{x},t)] = D(\mathbf{s},-t), \tag{3}$$

followed by an imaging condition which extracts the image as the wavefield at zero time:

$$R(\mathbf{x}) = W(\mathbf{x},t=0). \tag{4}$$

In this expression, the imaging velocity $v(\mathbf{x})$ is equal to half of the medium velocity. The wave operator $\mathbf{L}$ is the same as the one defined in Eq. 1, and the "–" sign on the source side indicates propagation backward in time.

The assumption that propagation from the sources to the reflectors and back to the receivers occurs on identical paths highlights an important limitation of imaging using zero-offset data. Implied in the stated assumption is that models are spatially invariant such that multi-pathing does not occur. (Multi-pathing means that waves propagate between two individual points in the medium along several



(a) Zero–offset data (b) Exploding reflector data

Fig. 1. A schematic representation of the exploding reflector model. (a) In the physical experiment, waves propagate from the source to the reflectors and back to the receivers along the same path. (b) The zero offset experiment can be recast equivalently assuming that the reflectors act as sources of energy at time zero (the reflectors "explode"), but waves propagate in a medium at half the speed of the original experiment. Figure adapted after Clærbout (1985).

trajectories, usually as a result of strong velocity gradient.) This assumption fails for asteroid models consisting of solid blocks of rock, surrounded by loose regolith material, whose properties differ by as much as 100%.

In summary, although one of the fastest imaging methods, zero-offset imaging of data subject to multi-pathing leads to artifacts with strength and geometry comparable with that of real reflectors. This can lead to inaccurate interpretation, especially for complex subsurface models. Moreover, it is very difficult to estimate an accurate velocity model using just zero-offset images. Another class of experiments using sources and receivers located at different positions relative to one-another addresses these drawbacks.

2.2. Multi-offset experiments

Multi-offset data are acquired using systems with separated transmitters and receivers. Data can be acquired using variable separation between the antennas, i.e. with variable offset. Wavefield imaging with multi-offset experiments is based on the assumption of single scattering at discontinuities in the subsurface (Berkhout, 1982; Clærbout, 1985). Under this assumption, waves propagate from the sources, interact with discontinuities inside the object under investigation and return to the receivers as reflected waves. The sources and receivers are separated by variable distance which ensures imaging along different propagation paths, i.e. different illumination directions.

In this framework, we commonly speak about a *source wavefield*, originating at the source and propagating in the medium prior to any interaction with discontinuities, and a *receiver wavefield*, originating at discontinuities and propagating in the medium to the receivers (Berkhout, 1982; Clærbout, 1985). The two wavefields coincide kinematically at discontinuities, a property which is usually measured by evaluating the zero-lag of the temporal cross-correlation between the two wavefields. Any mismatch between the wavefields indicates inaccurate wavefield reconstruction typically assumed to be due to inaccurate model parameters, the propagation velocity in this case. We do not need to make additional assumptions about how we reconstruct those two wavefields as long as the wave-equation used for wavefield reconstruction accurately describes wave propagation in the medium under consideration.

The source and receiver wavefields, W_s and W_r, are reconstructed using the same wave-equation and medium parameters, except that propagation is forward and backward in time, respectively:

$$\mathbf{L}(v)[W_s(\mathbf{x},t)] = D_s(\mathbf{s},+t) \tag{5}$$

$$\mathbf{L}(v)[W_r(\mathbf{x},t)] = D_r(\mathbf{r},-t) \tag{6}$$

In this expression, the imaging velocity $v(\mathbf{x})$ is equal to the actual medium velocity and the $+$ or $-$ signs in the source term indicates propagation forward or backward in time, respectively. A conventional cross-correlation imaging condition based on the reconstructed wavefields can be written as (Clærbout, 1985):

$$R_e(\mathbf{x}) = \sum_t W_s(\mathbf{x},t) W_r(\mathbf{x},t). \tag{7}$$

When multiple (N_e) experiments are used for imaging, the final image is simply the sum of all partial images corresponding to individual experiments:

$$R(\mathbf{x}) = \sum_{e=1}^{N_e} R_e(\mathbf{x}). \tag{8}$$

As is the case for zero-offset imaging in complex media characterized by multi-pathing, multi-offset imaging for individual experiments, i.e. the image R_e for experiment e, contains reflector information, as well as coherent artifacts due to correlation between waves propagating along crossing paths. However, the coherent artifacts seen in individual multi-offset images are inconsistent from one experiment to another. Summation over experiments, Eq. 8, reinforces the signal and attenuates the coherent noise, thus leading to cleaner and easier to interpret images than those obtained using zero-offset imaging. However, the cost of multi-offset acquisition and processing is significantly larger than the cost of processing zero-offset data. Nevertheless, the much higher image quality usually justifies the cost increase, as we show later in this paper.

We also note that the imaging condition shown in Eq. 7 is just one of many possibilities. We could, in principle, consider other imaging conditions that give us access to information about image accuracy, and implicitly about the accuracy of the velocity model. For example, a more

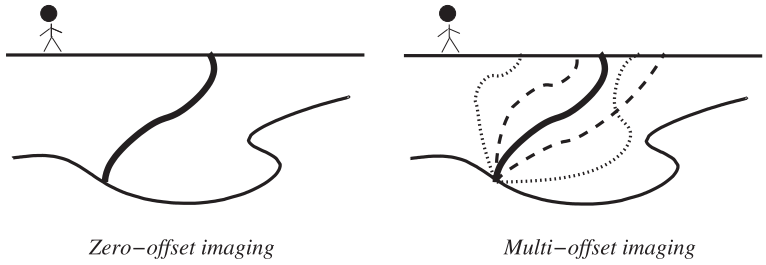


Fig. 2. Different experimental setups illuminate differently the subsurface: zero-offset – illumination at normal reflection angle, and multi-offset – illumination at many different reflection angles.

general imaging condition, also known as an extended imaging condition (Sava and Fomel, 2003; Sava and Vasconcelos, 2011), correlates the reconstructed source and receiver wavefields W_s and W_r:

$$R_e(\mathbf{x}, \boldsymbol{\lambda}, \tau) = \sum_t W_s(\mathbf{x} - \boldsymbol{\lambda}, t - \tau) W_r(\mathbf{x} + \boldsymbol{\lambda}, t + \tau), \tag{9}$$

followed by summation over experiments

$$R(\mathbf{x}, \boldsymbol{\lambda}, \tau) = \sum_{e=1}^{N_e} R_e(\mathbf{x}, \boldsymbol{\lambda}, \tau). \tag{10}$$

Here, $\boldsymbol{\lambda} = \{\lambda_x, \lambda_y, \lambda_z\}$ and τ are space- and time-shifts, respectively, that create systematic separation between the source and receiver wavefields, thus emphasizing the directionality and correlations between incident and reflected waves, (Sava and Fomel, 2003). This imaging condition allows us to evaluate the similarity between the images formed for different illumination directions, thus providing information that can be used to correct the model used for wavefield reconstruction (Sava and Biondi, 2004; Sava and Biondi, 2004).

2.3. Experimental setup comparison

The two classes of algorithms discussed in the preceding sections differ in several important aspects.

1. An important distinction between the algorithms used for zero-offset and multi-offset experiments arises from the illumination diversity characterizing acquisition with separated transmitters and receivers. By construction, the multi-offset experiments generate information at a given image position from many different directions of illumination. This reduces the possibility that a given reflector is placed in a shadow zone caused by structures that deflect waves propagating from the source or toward the receivers. In contrast, zero-offset experiments illuminate a given point in the subsurface along a single path that, in theory, corresponds to the normal incidence at the reflector, Fig. 2. The increased illumination diversity enables multi-offset experiments to produce higher quality images than those obtained with zero-offset experiments.

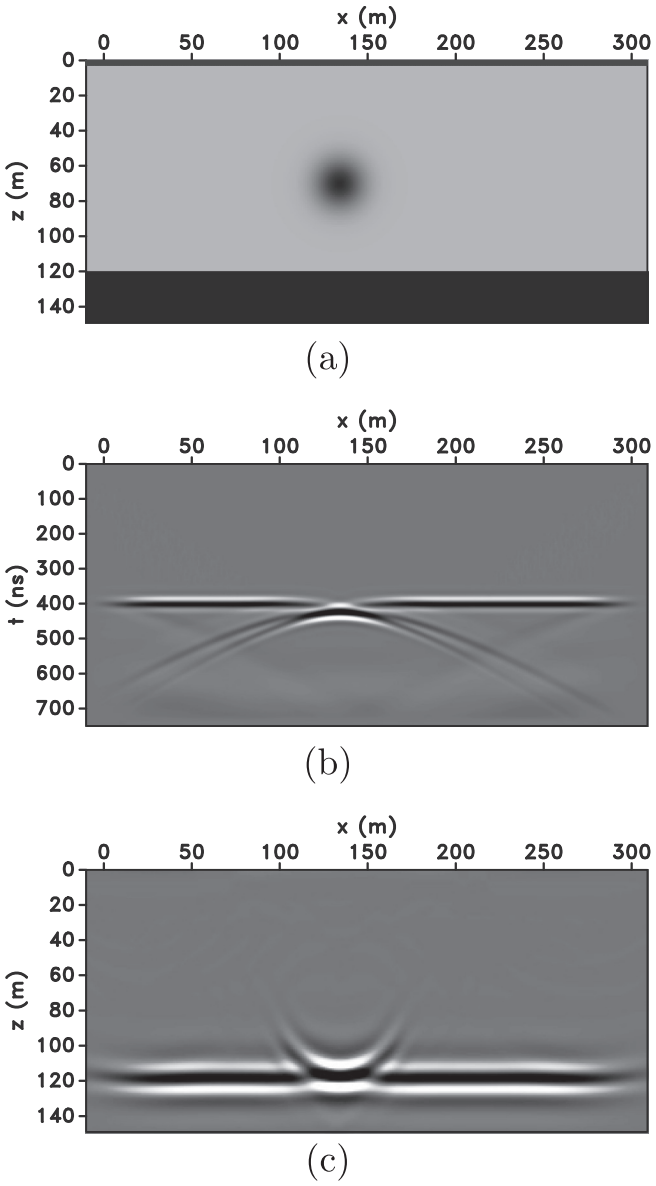


Fig. 3. Synthetic model illustrating artifacts caused by multi-pathing in zero-offset imaging. (a) Velocity with a low-velocity anomaly and a horizontal reflector, (b) zero- offset data and (c) zero-offset image.

2. A second consideration, is that multi-offset data allows attenuation of artifacts caused by multi-pathing. As indicated earlier, zero-offset imaging assumes that

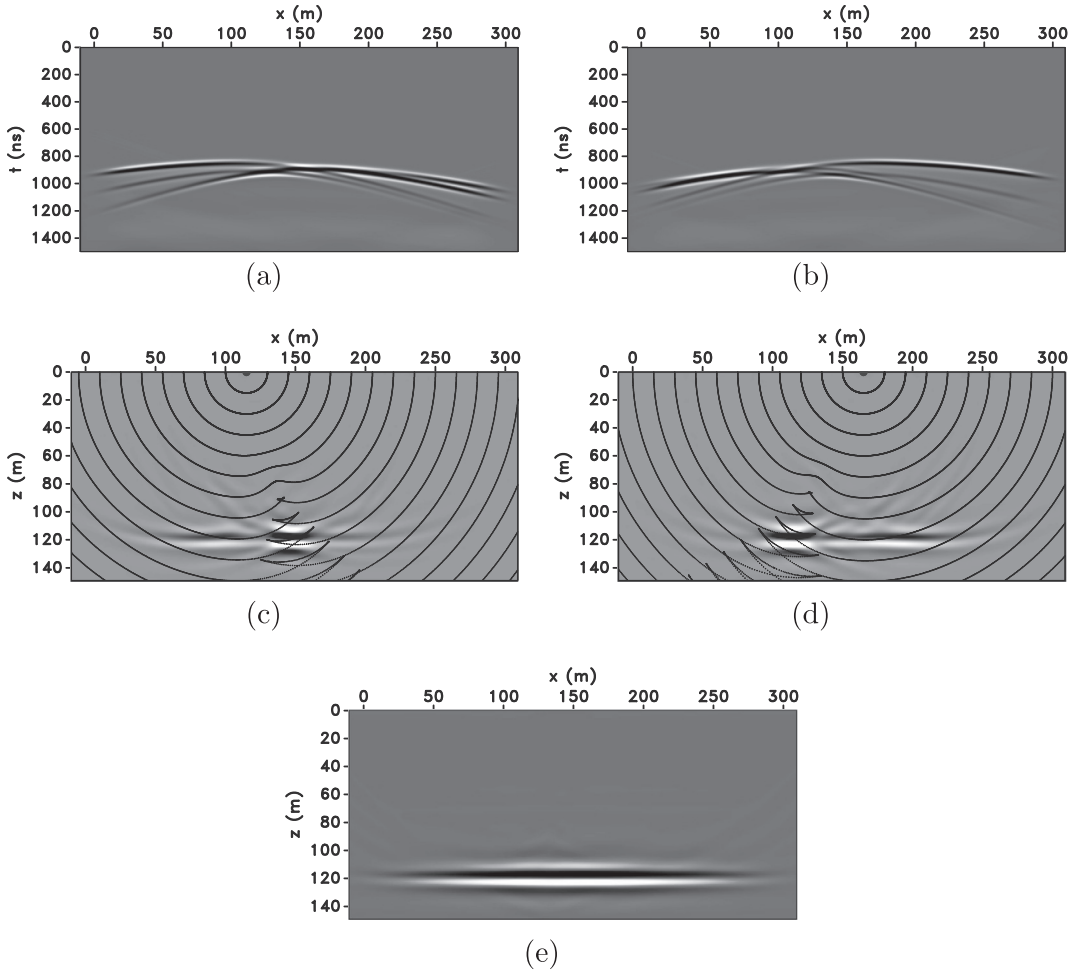


Fig. 4. Synthetic model illustrating multi-pathing artifact cancellation in multi-offset imaging. (a)-(b) Data for transmitters at different locations on the surface; (c)-(d) individual multi-offset images for the data shown in (a)-(b), respectively and (e) multi-offset image stack obtained by summing many individual images like the ones shown in (c)-(d).

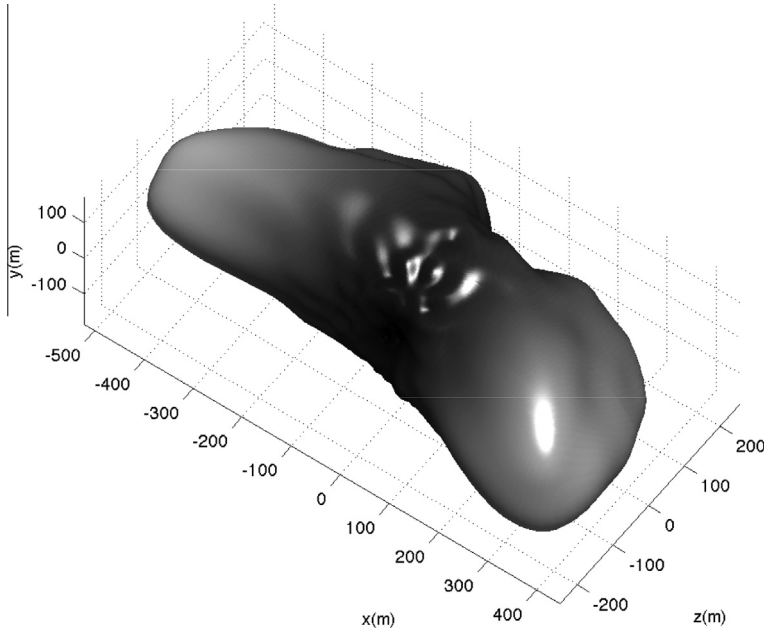


Fig. 5. Model based on the shape of asteroid 433 Eros. The asteroid interior consists of rock fragments surrounded by loose regolith material, Fig. 6. The gray shading indicates radial distance from a conventional center point inside the asteroid.

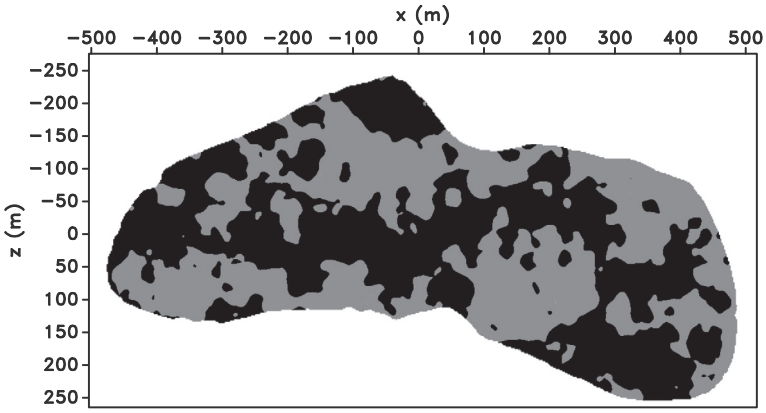


Fig. 6. Velocity model representing two different materials: rock (black) and regolith (gray), surrounded by empty space (white). The wave speeds in the three regions are 0.11 m/ns, 0.22 m/ns and 0.30 m/ns, respectively.

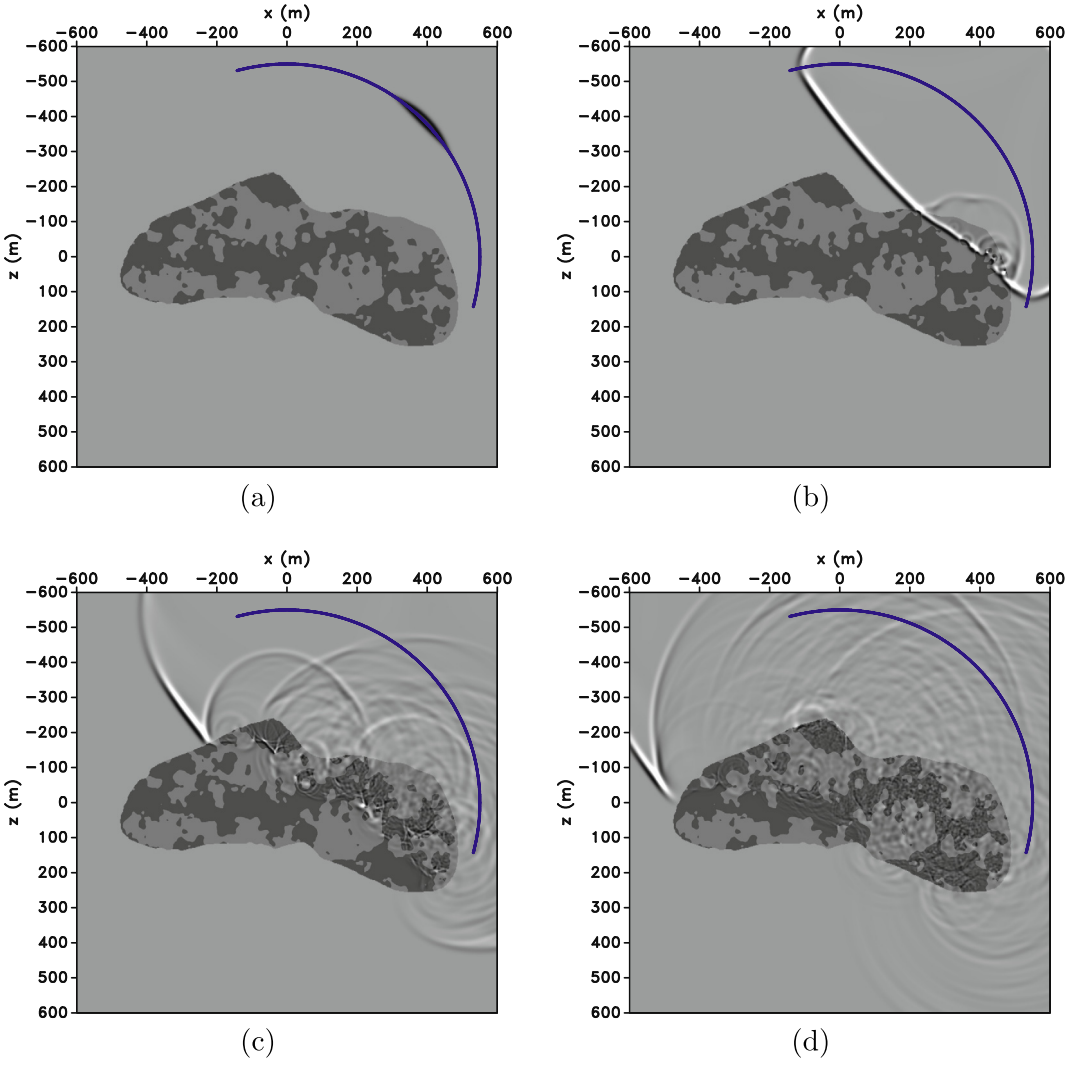


Fig. 7. Successive snapshots as a function of time for a wavefield simulated using finite-differences in the heterogeneous asteroid model. Panels (a)-(d) depict the model overlain by the wavefield at different times. The panels correspond to a single source located far from the asteroid, therefore the electromagnetic wave impinging on the asteroid is nearly planar, as seen best in panel (b).

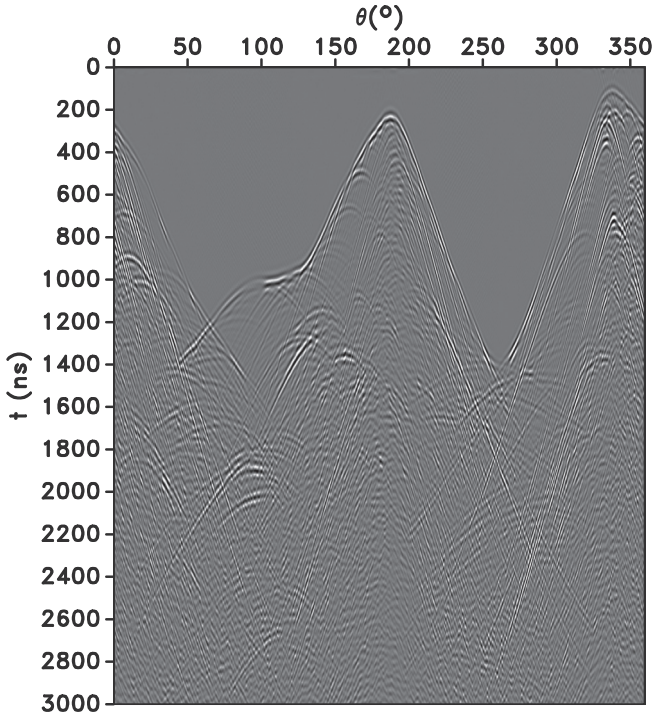


Fig. 8. Zero-offset data as a function of angle along a circular array around the asteroid. A fixed time delay corresponding to the propagation from the orbiter to a circular array around the asteroid and back to the orbiter is removed from the figure, for better visualization of the data.

propagation from the sources to receivers occurs on identical paths, which is not the case for models with significant velocity variation. In contrast, multi-offset imaging can attenuate such coherent artifacts because they are inconsistent from one experiment to another. Stacking over experiment attenuates the artifacts and reinforces the real reflectors. Figs. 3(a)-(c) and 4(a)-(e) illustrate this idea. For a simple reflector in a model with a low velocity anomaly (Fig. 3(a)), we can simulate the zero-offset data (Fig. 3(b)), from which we can construct the zero-offset image (Fig. 3(c)). In addition to the horizontal reflector (i.e. the signal), we can also see artifacts (i.e. the coherent noise) caused by wavefield multipathing. However, from multi-offset data for different transmitter positions (Fig. 4(a)-(b)), we can construct many multi-offset images (Fig. 4(c)-(d)), from which we obtain the stacked image (Fig. 4(e)). Since the artifacts (i.e. the coherent noise) are inconsistent from image to image, the stack attenuates the noise and reinforces the horizontal reflector (i.e. the signal). The multi-offset image has reduced coherent noise, unlike the zero-offset image. Such artifacts are numerous in a model characterized by many localized velocity anomalies which are responsible for wavefield multipathing.

3. A third consideration is that multi-offset experiments allow us to evaluate and improve the quality of the model used for imaging. The geologic structure inside the imaged object is invariant to the illumination direction, thus all experiments should locate a reflector at the same position. If this does not happen, we can conclude that the model is inaccurate, according to the so-called "semblance principle" (Yilmaz, 2001). Such analysis can be exploited for velocity model building using various techniques common in seismic exploration, e.g. through the use of the extended images discussed in Eq. 10.

We note that both zero-offset and multi-offset imaging lead to attenuation of incoherent (random) noise present in the data. We could, in principle, repeat a zero-offset survey N_e times and stack all images, thus achieving a signal-to-noise ratio improvement proportional to $\sqrt{N_e}$, which is similar to what we can obtain in multi-offset imaging by summation over the images obtained by separate experiments. However, this SNR improvement refers strictly to *random* noise and does not have any impact on the *coherent* noise discussed earlier.

We thus conclude that multi-offset imaging has significant advantages over single-offset imaging, albeit at a higher acquisition and processing cost. In the following

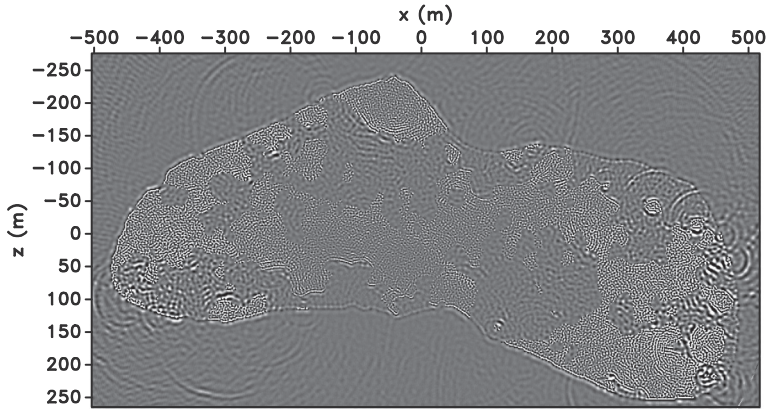


Fig. 9. Image obtained by wavefield-based migration using the zero-offset data shown in Fig. 8 and the correct velocity of the interior of the asteroid shown in Fig. 6.

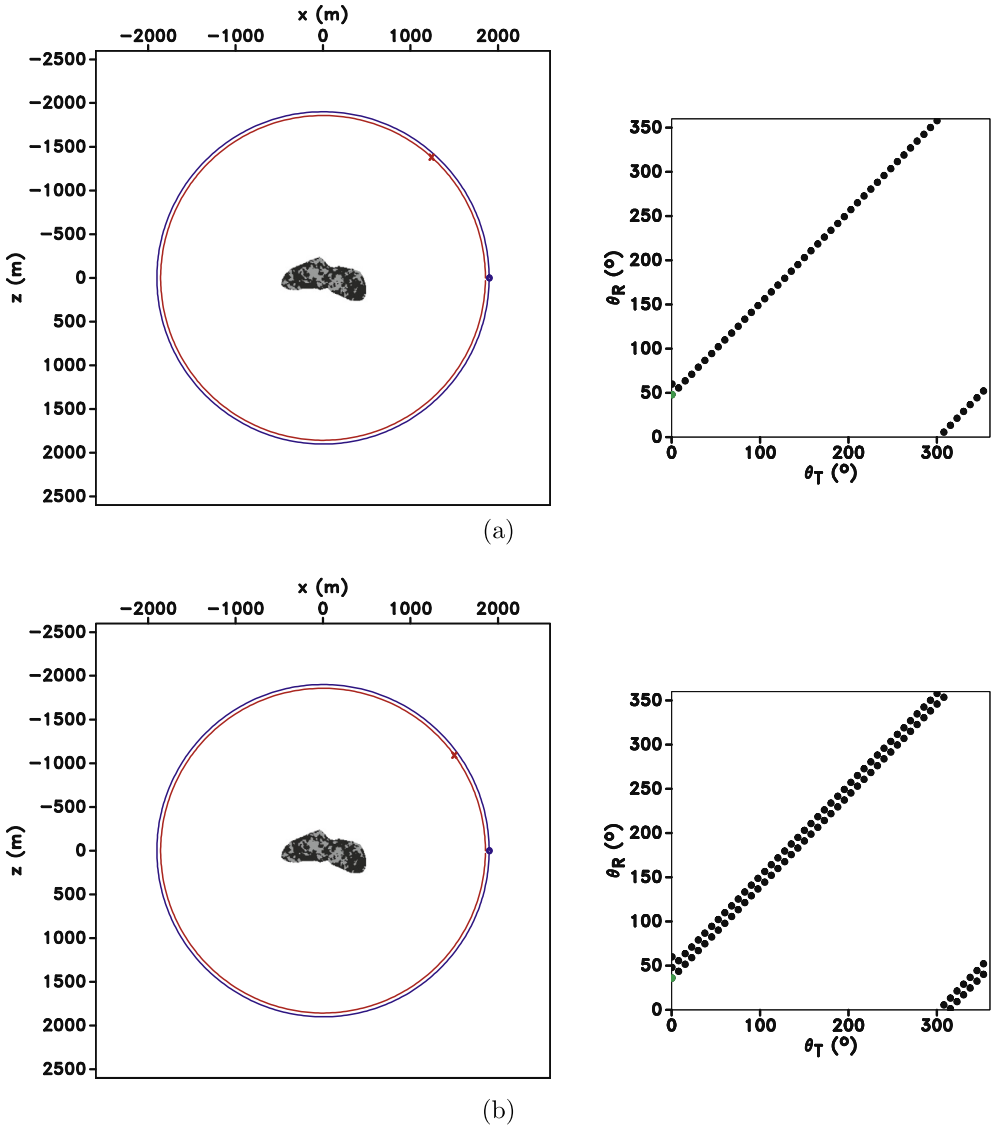


Fig. 10. Illustration of asynchronous radar acquisition using two orbiters. The left panels depict the positions of the transmitter and receiver orbiters relative to the asteroid, and the right panels in each frame show the positions occupied by the orbiters as a function of time.

section, we demonstrate the advantages of using multi-offset geometry for imaging inside a space object, asteroid or comet, with dual-orbiter radar systems.

3. Acquisition

Orbiter systems can be equipped with radar systems operating at multiple frequencies and revolving repeatedly around the target object. We assume that such orbiters carry radar antennas acting as transmitters and receivers of electromagnetic energy and show how such orbiters could be coordinated to generate multi-offset data. In the imaging section, we argue that such systems can deliver much higher imaging quality at a modest increase in acquisition and processing cost. In this section we outline how multiple orbiters can generate multi-offset data, although we do not discuss in great detail instrumentation or navigation parameters. Our focus is mainly on the imaging aspects and the improved image quality due to the higher data volume obtained using the dual orbiter setup. More details and a quantitative analysis of imaging results are provided by Grimm et al. (2014).

We begin with a demonstration of imaging using conventional acquisition with a single orbiter, and then proceed to the alternative acquisition geometry based on two orbiters.

3.1. Single orbiter

A conventional space-based radar acquisition system uses a single antenna which plays both the roles of transmitter and receiver of electromagnetic energy. Such instruments revolve repeatedly around the target object, and the transmitters are co-located with the receivers. This type of

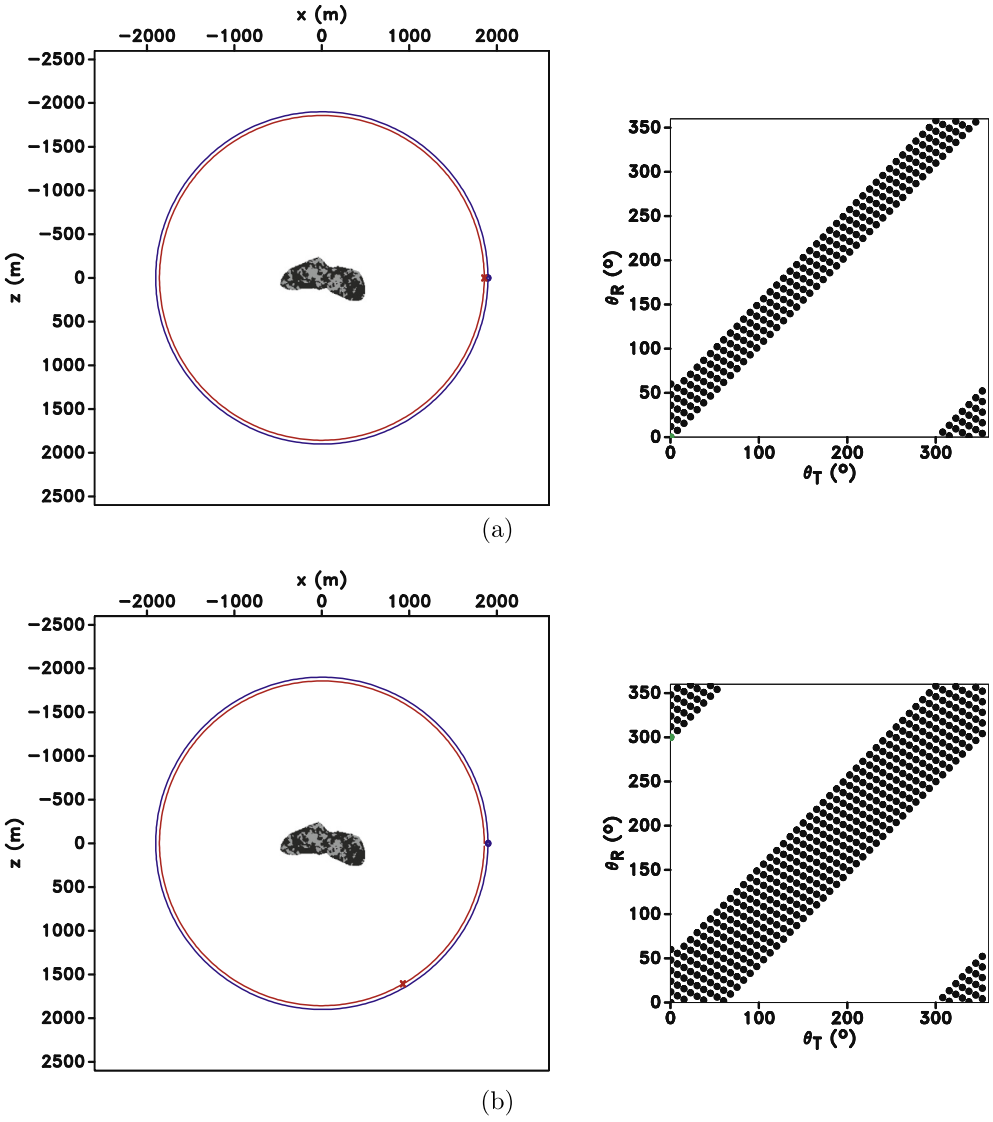


Fig. 11. Illustration of asynchronous radar acquisition using two orbiters. The left panels depict the positions of the transmitter and receiver orbiters relative to the asteroid, and the right panels in each frame show the positions occupied by the orbiters as a function of time.

acquisition is akin of the zero-offset acquisition in terrestrial seismic exploration or of common ground-penetrating radar (GPR) systems.

Electromagnetic waves emitted by the source propagate without attenuation in the empty space between the orbiter and the target (asteroid, comet, etc) and back. Such waves also penetrate inside the object where they are attenuated and propagate for a distance which depends on its dielectric properties and then reflect at locations where the physical properties change abruptly. Thus, reflected electromagnetic energy can be used to map the discontinuities in the subsurface using zero-offset imaging techniques. Such images suffer from the drawbacks discussed earlier, i.e. poor illumination and multi-pathing artifacts.

We illustrate this method with a model based on the shape of asteroid 433 Eros (Gaskell, 2008), but scaled down in order to represent a typical NEA, Fig. 5. Our model consists of a combination of a rock fragments surrounded by loose regolith material (Richardson et al., 2002; Weissman et al., 2004). The interior structure is arbitrary and it is used here only for imaging assessment. In the following numeric experiments, we simulate waves for a two-dimensional slice through this model, Fig. 6. Similar experiments could be performed in three dimensions; we do not discuss these more computationally intensive experiments here, but we note that the methodology discussed here can be extended without theoretical restrictions.

We consider an orbiter around this object at a distance of 2.5 km from the asteroid's center. The numeric experiments consist of the following steps:

1. Use analytic Green's functions to relocate the source function (Ricker wavelet) from the transmitter antenna, to a fictitious surface in close proximity of the asteroid

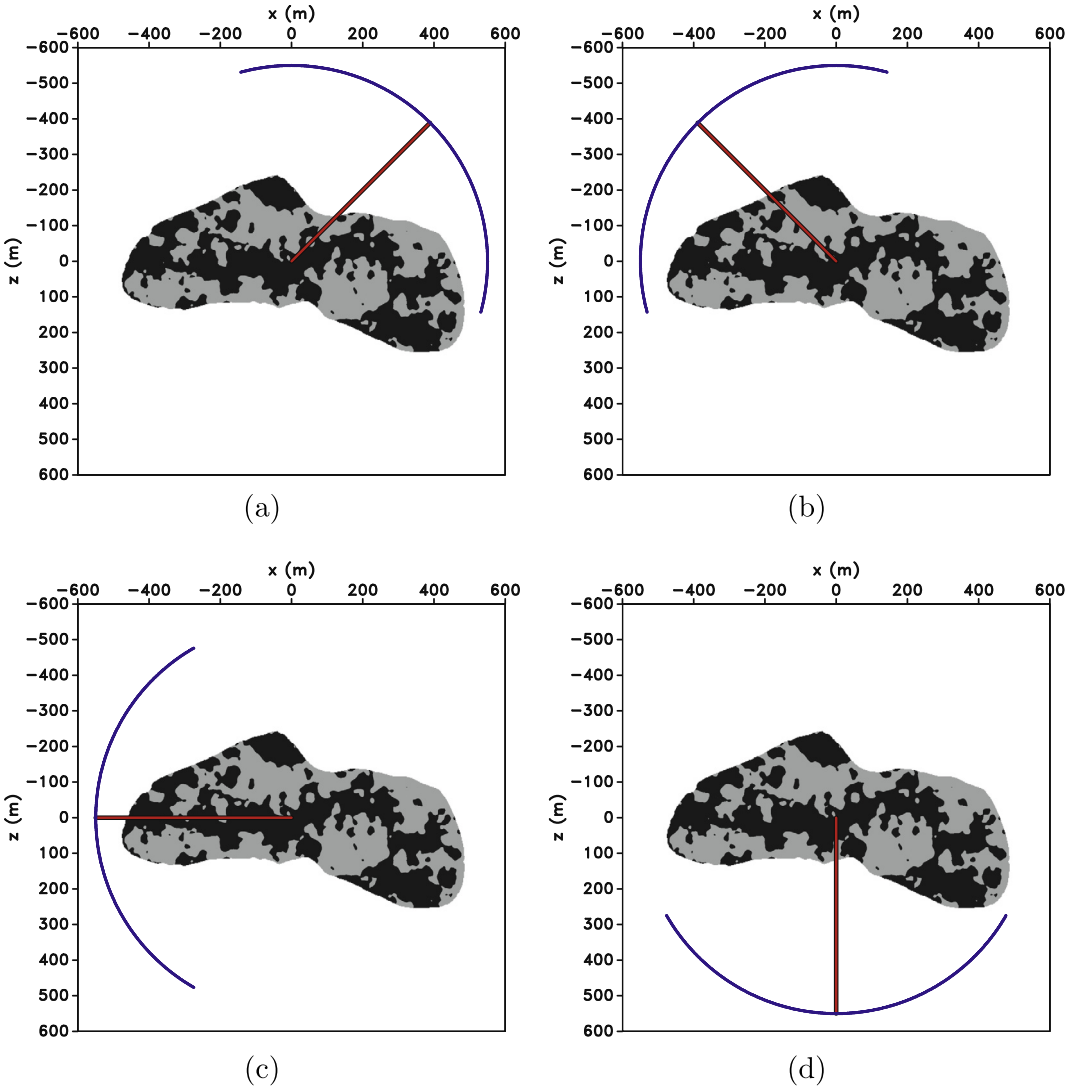


Fig. 12. Acquisition geometry for a transmitter at (a) 45°, (b) 135°, (c) 180° and (d) 270°. The blue arc indicates schematically the effective aperture, and the red lines point toward the transmitter antenna. The actual transmitter and receiver orbiters are assumed to be at 2.5 km from the center of the asteroid.

(i.e. a circular contour at 0.55 km from the center of the asteroid). This is a fast operation and we perform it in order to reduce the compute time of the following steps.

2. Use time-domain finite-difference modeling starting with the source relocated at the fictitious circular surface to simulate waves propagating inside the asteroid and reflecting back outside the model; then collect data on the same fictitious circular surface.
3. Use analytic Green's functions to relocate the observed wavefield from the fictitious circular surface to the receiver antenna which is co-located with the transmitter antenna.

This procedure ensures that we use the fastest propagation method in the void space separating the true orbiter trajectory and the fictitious surface in the vicinity of the asteroid, and that we use an accurate method to simulate waves propagating inside the asteroid.

Figs. 7(a)-(d) show different snapshots of the wavefield superimposed on the asteroid model. The highly scattering materials lead to complex wavefields characterized by multi-pathing and repeated scattering inside the asteroid. Accurate imaging inside the asteroid requires that we exploit fully such broadband and wide aperture wavefields, e.g. we use techniques like reverse-time migration (RTM).

The recorded data as a function of time and angle for sources located every 0.5° all around the asteroid is shown in Fig. 8. We can clearly notice the complexity of the reflections due to the heterogeneous model causing wavefield multi-pathing. Using zero-offset finite difference imaging as outlined earlier, we obtain the image shown in Fig. 9. This image gives a rough indication of the interfaces located inside the model, but does not produce a clear image of all discontinuities. This blurring is caused by the fact that much of the scattering associated with the heterogeneous interior of the asteroid is ignored simply because we collect data only at the receiver co-located with the transmitter. Additional repeat zero-offset datasets can reduce the random noise present in the data (e.g. instrument noise), but cannot attenuate the artifacts caused

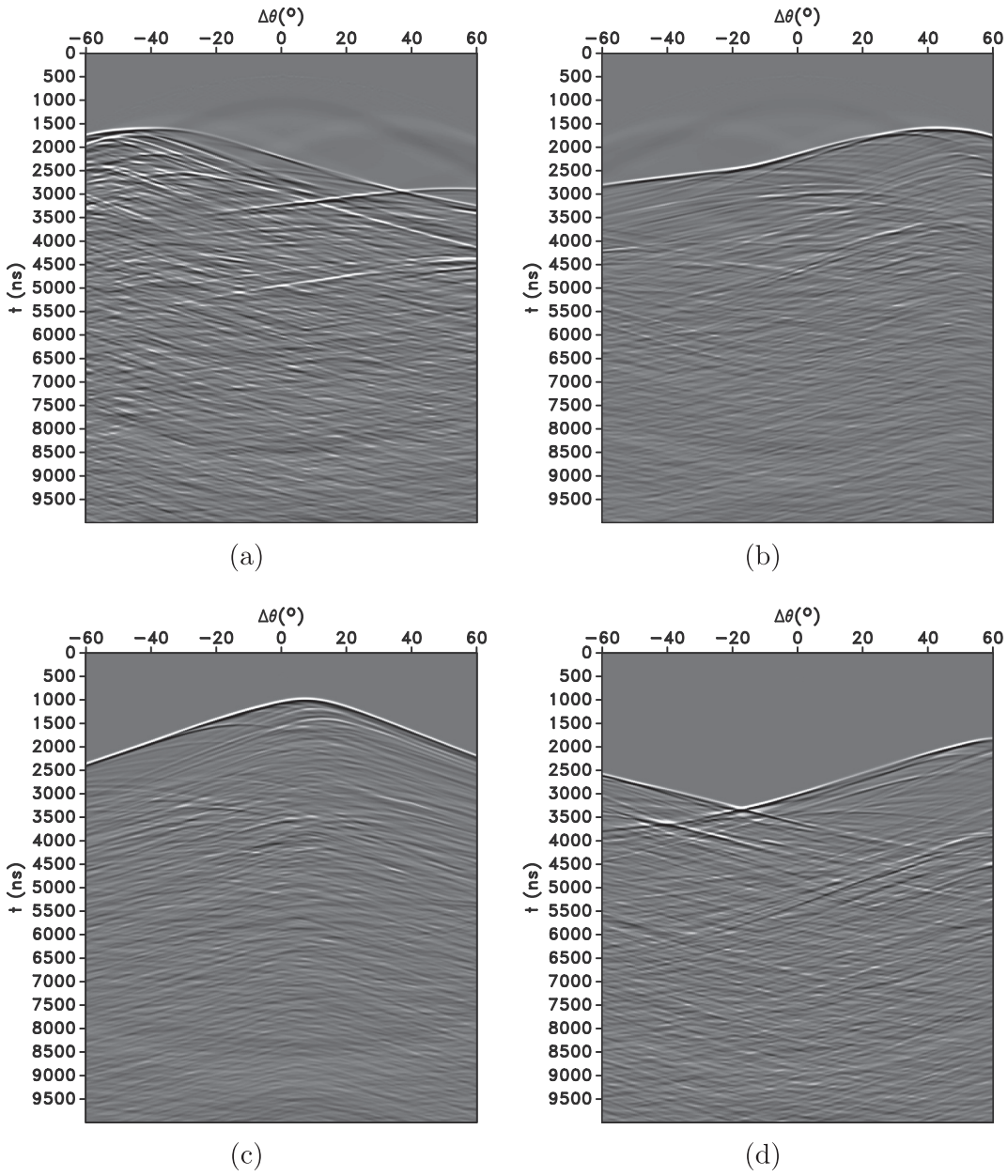


Fig. 13. Recorded data for the transmitter and receiver configuration shown in Fig. 12(a)-(d). The origin of the time axis is set to remove the delay corresponding to propagation from the transmitter to a fictitious surface in close proximity of the asteroid (i.e. a circular contour at 0.55 km from the center of the asteroid).

multi-pathing. An example of such artifacts can be seen in Fig. 9 at coordinate $x = 350$ m and $z = -75$ m; some reflectors in this region do not correspond to true geologic interfaces.

3.2. Dual orbiter

Improved imaging can be performed using a different acquisition setup involving data observed at multiple receivers for a pulse emitted from a single transmitter. In conventional ground-based seismic exploration, this is done by laying on the ground massive receiver arrays characterized by long transmitter–receiver separation at all azimuths. This is, of course, not possible for systems in orbit around a small object like an asteroid.

Our proposed solution is the following: instead of co-locating the transmitter and receiver antennas on the same orbiter, we advocate the use of separate orbiters for the two antennas. In this setup, each orbiter is placed on a different trajectory around the asteroid, thus insuring different orbital revolution speeds. The relative speed between the transmitter and receiver orbiters can be adjusted easily by changing the orbiter elevation relative to the asteroid.

The net effect is that the angular separation between the transmitter and receiver orbiters changes permanently, thus providing data with a variable separation (offset) as a

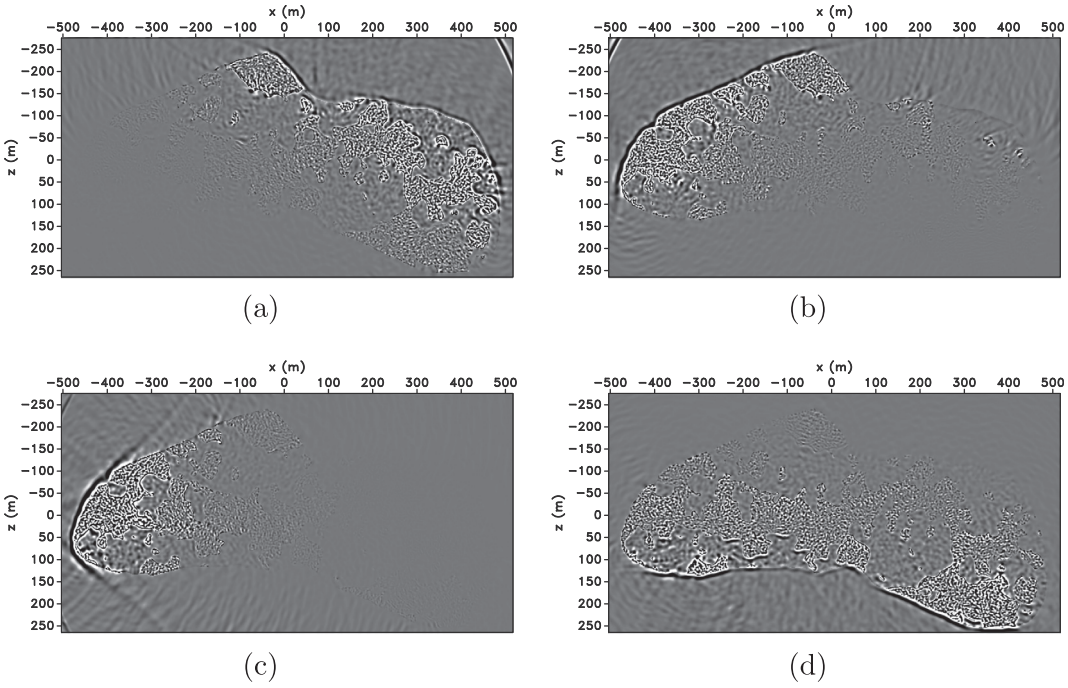


Fig. 14. Partial images constructed using the data shown in Fig. 13(a)-(d).

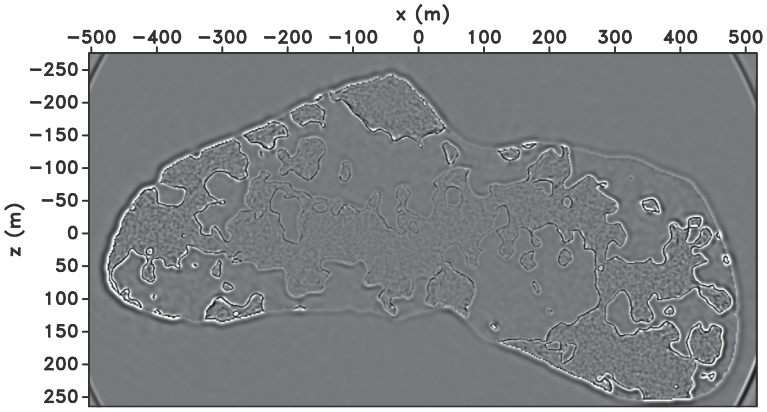


Fig. 15. Multi-offset image obtained by stacking all partial images like the ones shown in Fig. 14(a)-(d). The inside of the asteroid is more weakly imaged due to the limited acquisition time, which effectively truncates data that arrives from deeper in the asteroid.

function of time. After many orbits, the transmitter orbiter returns repeatedly to a given position; each time, however, the receiver orbiter is at a different position with respect to the transmitter orbiter. The data corresponding to different transmitter–receiver separations can be sorted to construct the equivalent of "shot gathers" from conventional seismic exploration, i.e. data corresponding to a fixed transmitter position, but with receivers located at different distances (offsets) from the source. Time redundancy, therefore, allows us to collect multi-offset data using only two separate orbiters around the asteroid. The longer the orbiters collect data the more illumination angles and the better the resulting image; more orbiters speed-up acquisition time.

We illustrate this method with the same model shown in Fig. 5. Figs. 10(a)-11(b) show how we can gradually build redundant data with aperture from $\pm 60^\circ$ using two asynchronous orbiters. We consider transmitter and receiver orbiters making full revolutions in slightly different periods. Each frame depicts on the left the position of the two orbiters at various times, and on the right the angular coverage as a function of transmitter and receiver angles accumulated over time. Due to its quicker revolutions, the receiver orbiter gradually catches up with the transmitter orbiter and then takes over. In this example, the receiver orbiter starts 60° behind the transmitter orbiter, and ends 60° ahead. Figs. 13(a)-(d) show the data obtained after sorting the observed wavefields for fixed transmitter posi-

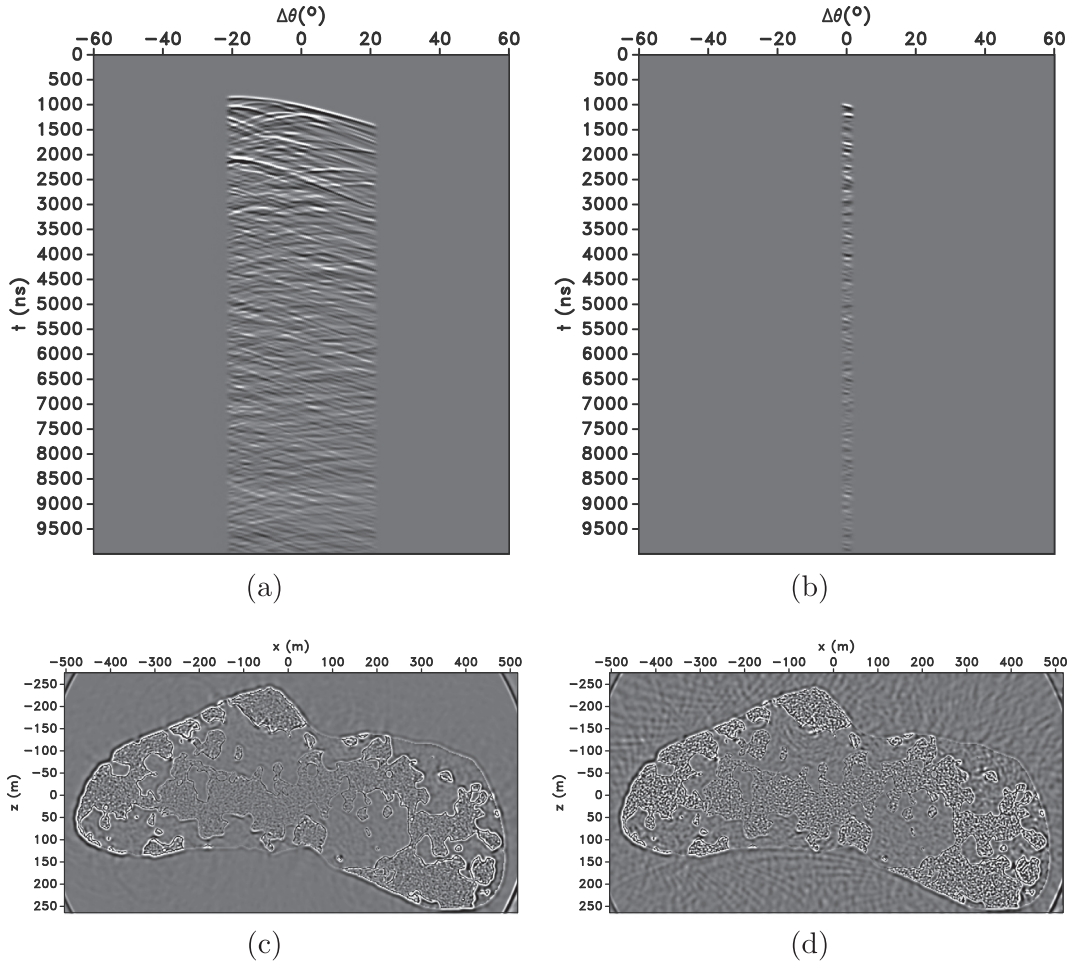


Fig. 16. Image quality dependence as a function of effective aperture: data for one multi-offset experiment with (a) ±20° and (b) ±2° aperture; migrated images for all multi-offset experiments with (c) ±20° and (d) ±2° aperture. As aperture decreases, the image becomes noisier and the interior reflectors become less focused and gets contaminated by artifacts. The truncation artifacts present in these images can obstruct the similar information present in the full-aperture image, Fig. 15.

tions (at angles of $45°, 135°, 180°$ and $270°$ relative to an arbitrary point on the orbit).

Similarly to the zero-offset data shown in Fig. 8, the multi-offset data captures the complexity of the model. However, this acquisition style gives us access to much more detailed information about the scattered wavefield, despite the fact we are still not using full receiver aperture around the asteroid. Figs. 12(a)-(d) depict the effective receiver aperture constructed around the asteroid for different positions of the source. Figs. 14(a)-(d) depict partial images obtained by multi-offset wavefield-based imaging for the data shown in Figs. 13(a)-(d), respectively, and with the correct velocity model shown in Fig. 6. Each multi-offset dataset images a different portion of the model, corresponding to the position of the transmitter antenna. The quality of each partial multi-offset image is comparable with the quality of the zero-offset image, Fig. 9, aside from the reduced aperture due to the finite number of revolutions executed by the two orbiters. In this experiment, we repeat multi-offset imaging with transmitters at every 3° and with receivers at every 1° between ±60° relative to the transmitter. Although we do not use any attenuation in this example, the far side of the asteroid (opposite the position of the transmitter) is not illuminated due both to the limited aperture, and to the finite acquisition time. However, the aperture and acquisition time parameters can be controlled, thus opening the possibility to image deep into the asteroid and from multiple angles.

Finally, the image shown in Fig. 15 depicts the sum of all partial images, according to Eq. 8. Compared to the zero-offset image, Fig. 9, the multi-offset image is of much better quality; the interior interfaces are clearly defined and correctly positioned in the model, and the coherent artifacts are attenuated, thus providing a better opportunity to interpret the geologic structure of the asteroid interior.

4. Discussion

Several challenges posed by radar imaging in comets and asteroids remain to be addressed in the future:

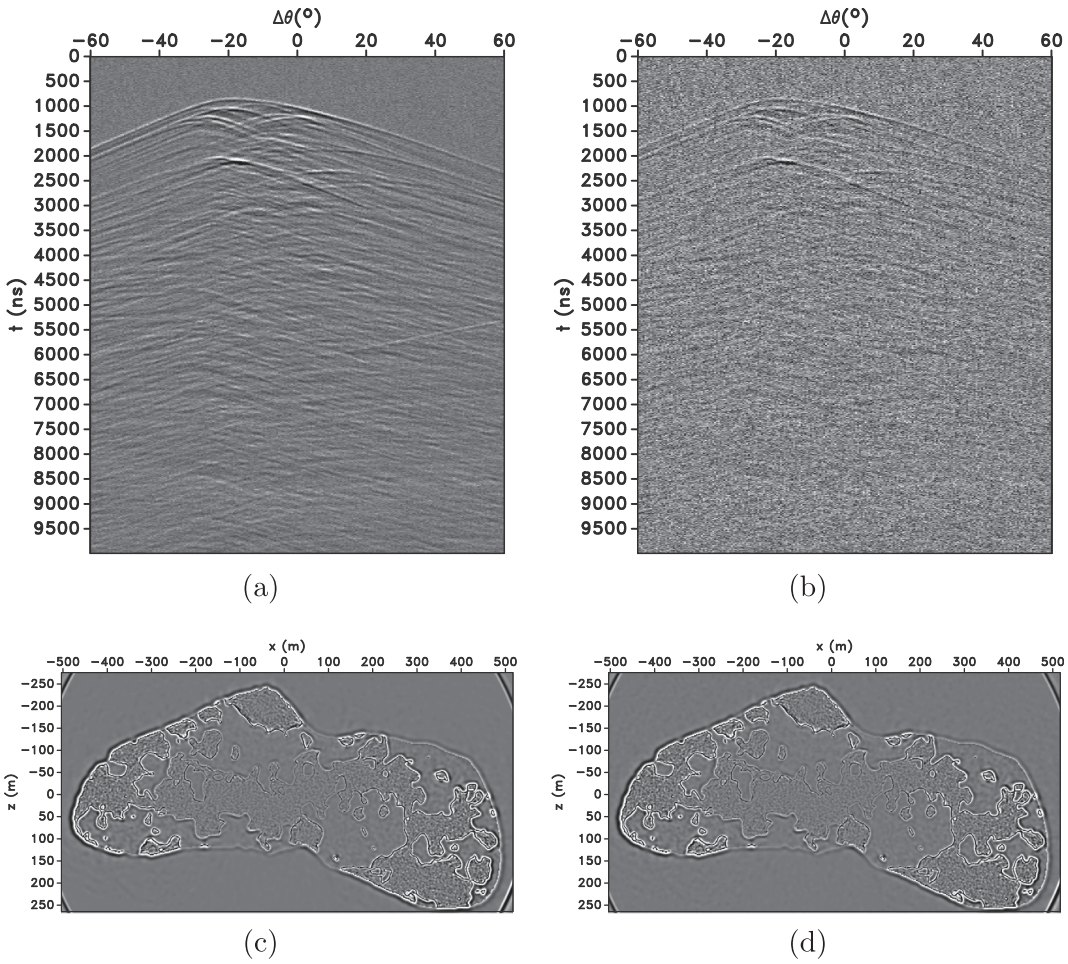


Fig. 17. Image quality dependence as a function of random noise level: data for one multi-offset experiment with (a) −20 dB and (b) −10 dB random noise; migrated images for all multi-offset experiments with (c) −20 dB and (d) −10 dB random noise. Panel (b) exaggerates any expected instrument noise, but it is shown here as a worst-case scenario test. The images reveal similar information as seen in the noise-free image, Fig. 15.

- How important is it to define a good quality velocity model for imaging? How strongly does attenuation influence the depth of penetration inside the asteroid, as a function of lithology?
- How robust is our methodology to large and incoherent instrument noise?
- How important is to simulate data with more accurate physics, in particular to take polarization into account?
- What are the optimal navigation parameters to maximize 3D coverage and speed up acquisition of multi-offset data?

We do not discuss these questions in detail here, aside from the aperture and noise issues which fit in the scope of our paper. The model accuracy and attenuation questions are addressed by Grimm et al., 2014.

In our acquisition setup, the multi-offset experiment aperture depends on the acquisition duration, i.e. the total number of revolutions around the asteroid. Shorter acquisition time reduces the effective aperture of the surveys, which in turn degrades the image accuracy. Figs. 16(c)-(d) illustrate this idea. The different panels correspond to apertures of $\pm 20^\circ$ and $\pm 2^\circ$, respectively. The image degrades for smaller aperture and becomes noisier, approaching in the limit the zero-offset image quality, Fig. 9. The artifacts contaminating the images produced with smaller aperture cannot be attenuated by repeating the same experiments, but only by adding other experiments that provide coverage from additional directions, i.e. offsets.

Different types of noise can corrupt reflected data observed at the orbiter. As discussed earlier, correlated noise can masquerade as real signal and lead to spurious events in the image. This is similar to the case of seismic or GPR surveys where multiple reflections or mode conversions overlap with primary, pure mode reflections. Here we assume that such correlated noise is negligible and does not corrupt the observed data. However, we assume that the instrument itself, i.e. the radar antenna, can introduce noise into the data. Such noise is best modeled as a random signal with a normal distribution, and its main characteristic is its strength relative to the observed signal. Figs. 17(a)-(b) show multi-offset data for a single experiment (i.e. a fixed location of the transmitter antenna) with

signal-to-noise ratios of −20 dB and −10 dB, respectively. We assume that all such gathers are corrupted by noise with the same levels, and the same distributions. Although the random noise is clearly visible in the data, the migrated images, Fig. 17(c)-(d) indicate that such uncorrelated noise does not leave a significant imprint on the images and that the information about the major interfaces inside the asteroid is essentially identical with what we could obtain using noise-free data, Fig. 15. We conclude that the methodology discussed here is robust with respect to instrument noise characterizing available instrumentation.

We also note that in this paper we concentrate primarily on imaging using back-scattered energy, i.e. waves returning to receivers located in the vicinity of the transmitters. This setup is similar to the one used in surface seismic exploration in which case both sources and receivers have to be placed on the same side of the imaged volume, i.e. on the surface. However, the dual orbiter setup offers the possibility to collect data at receivers located on the opposite side of the transmitter relative to the asteroid. In this case, we can use the recorded data in transmission mode to infer the physical properties of the asteroid, e.g. by wavefield tomography. This setup is similar to the one used in cross-well seismic tomography.

An important consideration in the quality of the migrated image is the accuracy of the model used for wavefield reconstruction, according to Eq. 1. Of all factors influencing the imaging quality, the accuracy of the velocity model turns out to make the largest impact, as discussed in detail by Grimm et al. (2014). In general, the velocity model inside the asteroid is not known a priori and has to be determined in an iterative tomographic process akin to the well-known waveform inversion. Wavefield tomography can also be performed in transmission or reflection mode, therefore the data necessary for model building is identical to the data needed for wavefield imaging. However, wavefield tomography (Tarantola, 1984; Pratt and Worthington, 1990; Plessix, 2006) requires images constructed with different multi-offset experiments (the "semblance principle"), which further emphasizes the benefits of acquisition with a dual-orbiter system.

Finally, radar resolution is commonly improved using a synthetic aperture, and the techniques used in this paper have some analogy with the delay-and-sum approach to beamforming. It is worth noting here that classical Doppler methods are ineffective for small bodies due to the very low speeds involved. Spacecraft orbital velocities are just tens of cm/s, which requires ~ 1000 s to synthesize apertures of hundreds of meters. This vastly exceeds the ~ 1 s integration times of air- and space-borne SARs. Relative velocities due to target-body rotation are just as small, also obviating useful Doppler bandwidth.

5. Conclusions

Imaging the interior of highly complex asteroid or comet interiors is possible using orbital radar systems. Accurate imaging depends on our ability to use broadband electromagnetic wavefield data with large angular aperture. Such data can be acquired using pairs of spacecrafts orbiting repeatedly and at different distances around the imaged object. Data collected at different angular apertures can be sorted to create virtual multi-offset experiments which can be imaged using conventional wavefield-based methods. In contrast with more conventional zero-offset acquisition systems, multi-offset systems provide coverage of the target from many directions, thus improving image quality (better illumination, fewer coherent image artifacts) and providing appropriate data that can be used to infer model parameters through wavefield tomography.

Acknowledgments

This work was supported in part by the NASA Planetary Instrument Definition and Development Program, Grant No. NNX11AJ50G and by the sponsors of the Center for Wave Phenomena at Colorado School of Mines. The reproducible numeric examples in this paper use the Madagascar open-source software package freely available from http://www.ahay.org This research was supported in part by the Golden Energy Computing Organization at the Colorado School of Mines using resources acquired with financial assistance from the National Science Foundation and the National Renewable Energy Laboratory.

References

Aki, K., Richards, P., 2002. Quantitative Seismology,, University Science Books.

Asphaug, E., Barucci, A., Belton, M., Bhaskaran, S., Brownlee, D., Carter, L., Castillo, J., Chelsey, S., Chodas, P., Farnham, T., Gaskell, R., Gim, Y., Heggy, E., Klaasen, K., Kofman, W., Krelavsky, M., Lisse, C., MxFadden, L., Pettinelli, E., Plaut, J., Scheeres, D., Turtle, E., Weissman, P., Wu, R., 2010. Deep Inter. Radar Imaging Comets, 2670.

Asphaug, E., Ryan, E., Zuber, M., 2004. Asteroid interiors. In: Asteroids III. University of Arizona Press.

Barriot, J., Kofman, W., Henrique, A., Leblanc, S., Portal, A., 1999. A two dimensional simulation of the Consert experiment (radio tomography of comet Wirtane). Adv. Space Res. 24, 1127–1138.

Barucci, M.A., D'Arrigo, P., Ball, P., Doressoundiram, A., Dotto, E., Kofman, W., Orosei, R., Patzold, M., Perozzi, E., 2005. The ISHTAR mission: probing the internal structure of NEOs. In: Highlights of Astronomy, vol. 13. IAU SYMPOSIA.

Benna, M., Barriot, J., Kofman, W., Barbin, Y., 2004. Generation of 3-D synthetic data for the modeling of the CONSERT experiment (the radiotomography of comet 67P/ChuryumovGerasimenko). Antennas Prop. 52, 709–717.

Benna, M., Piot, A., Barriot, J., Kofman, W., 2002. Data set generation and inversion simulation of radio waves propagating through a two-dimensional comet nucleus (CONSERT experiment). W Radio Sci. 37.

Berkhout, A.J., 1982. Imaging of Acoustic Energy by Wave Field Extrapolation. Elsevier.

Bottke, W., Cellino, A., Paolicchi, P., Binzel, R., 2002. An overview of the asteroids: the Asteroids III perspective. In: Asteroids III. University of Arizona Press.

Brophy, J., Culick, F., Friedman, L., Allen, C., Baughman, D., Bellerose, J., Belts, B., Brown, M., Brush, M., Casani, J., Coradini, M., Dankanich, J., Dimotakis, P., Elvis, M., Garrick-Bethel, I., Gershman,

B., Jones, T.,Landau, D., Lewicki, C., Lewis, J., Llanos, P., Lupisella, M., Mazanek, D., Mehrotra, P., Nuth, J., Parkin, K., Schweickart, R., Singh, G., Strange, N., Tantardini, M., Wilcox, B., Williams, C., Williams, W., Yeomans,D., 2012. Asteroid retrieval feasibility study. Keck Inst. Space Studies, kiss.caltech.edu/study/asteroid/asteroid final report.pdf.

Carley, R., Heggy, E., 2008. Finite difference time domain simulation of radar wave propagation through comet nuclei dielectric models. Meteorit. Planet. Sci. 47, 1085–1095.

Chapman, C., 2004. The hazard of near-Earth asteroid impacts on Earth. Earth Planet. Sci. Lett. 222, 1–15.

Clærbout, J.F., 1985. Imaging the Earth's Interior. Blackwell Scientific Publications.

Festou, M., Kellera, H., Weaver, H., 2004. A brief conceptual history of cometary science. In: Comets II. University of Arizona Press.

Gaskell, R., 2008. Eros Shape Model V1.0. sbn.psi.edu/pds/resource/erosshape.html, NASA Planetary Data System.

Grimm, R., 2009. Electromagnetic sounding of solid planets and satellites. Decadal Survey White Paper.

Grimm, R., Stillman, D., Sava, P.C., Ittharat, D., 2014. Radio reflection imaging of asteroid and comet interiors II: Results and Recommendations. Adv. Space Res., submitted for publication.

Hilton, J., 2002. Asteroid masses and densities. In: Asteroids III. University of Arizona Press.

Huebner, W., Greenberg, J., 2001. Methods for determining material strengths and bulk properties of NEOs. Adv. Space Res. 28, 1129–1137.

Kofman, W., Herique, A., Goutail, J.-P., Hagfors, T., Williams, I.P., Nielsen, E., Barriot, J.-P., Barbin, Y., Elachi, C., Edenhofer, P., Levasseur-Regourd, A.-C., Plettemeier, D., Picardi, G., Seu, R., Svedhem, V., 2007. The comet nucleus sounding experiment by radiowave transmission (CONSERT): a short description of the instrument and of the commissioning stages. Space Sci. Rev. 128, 413–432.

Kofman, W., Safaeinili, A., 2004. Peering inside near-Earth objects with radio tomography. In: Mitigation of Hazardous Comets and Asteroids. Cam-bridge University Press.

Miller, R.D., Bradford, J.H., Holliger, K. (Eds.), 2010. Advances in Near-Surface Seismology and Ground-Penetrating Radar. Society of Exploration Geophysicists.

Picardi, G., Biccari, D., Seu, R., Plaut, J., Johnson, W., Jordan, R., Safaeinili, A., Gurnett, D., Huff, R., Orosei, R., Bombaci, O., Calabrese, D., Zampolini, E. 2004. MARSIS: Mars Advanced Radar for Subsurface and Ionosphere Sounding. In: Mars Express – The Scientific Payload ESA SP-1240, 51–69.

Plessix, R.-E., 2006. A review of the adjoint state method for computing the gradient of a functional with geophysical applications. Geophys. J. Int. 167, 495–503.

Pratt, R.G., Worthington, M.H., 1990. Inverse theory applied to multi-source cross-hole tomography. part 1: acoustic wave-equation method. Geophys. Prospect. 38 (03), 287–310.

Reynolds, J.M., 2011. An Introduction to Applied and Environmental Geo-physics,, Wiley.

Richardson, D., Leinhardt, Z., Melosh, H., Bottke, W., Asphaug, E., 2002. Gravitational aggregates: evidence and evolution. In: Asteroids III. University of Arizona Press.

Ricker, N., 1944. Wavelet functions and their polynomials. Geophysics 9 (3), 314–323.

Ricker, N., 1953. Wavelet contraction, wavelet expansion, and the control of seismic resolution. Geophysics 18 (4), 769–792.

Roark, S., Dissly, C.C.R., Scheeres, D., Petr, V., Housen, K., 2010. Explosive Surface Pods for Cratering Experiments on Small Bodies. In: Proceedings of the 41st Lunar and Planetary Science Conference. pp. 2100.

Safaeinili, A., Gulkis, S., Hofstadter, M., Jordsn, R., 2002. Probing the interior of asteroids and comets using radio reflection tomography. Meteorit. Planet. Sci. 37, 1953–1963.

Sava, P.C., Biondi, B., 2004. Wave-equation migration velocity analysis – I: theory. Geophys. Prospect. 52, 593–606.

Sava, P.C., Biondi, B., 2004. Wave-equation migration velocity analysis - II: subsalt imaging examples. Geophys. Prospect. 52, 607–623.

Sava, P.C., Fomel, S., 2003. Angle-domain common image gathers by wavefield continuation methods. Geophysics 68 (3), 1065–1074.

Sava, P.C., Vasconcelos, I., 2011. Extended imaging condition for wave-equation migration. Geophys. Prospect. 59 (1), 35–55.

Seu, R., Phillips, R., Biccari, D., Orosei, R., Masdea, A., Picardi, G., Safaeinili, A., Campbell, B., Plaut, J., Marinangeli, L., Smrekar, S., Nunes, D., 2007. SHARAD sounding radar on the Mars Reconnaissance Orbiter 112 (E5), n/a–n/a.

Sherriff, R.E., Geldart, L.P., 2010. Exploration Seismology. Cambridge University Press.

Tarantola, A., 1984. Inversion of seismic reflection data in the acoustic approximation. Geophysics 49 (08), 1259–1266.

Walker, J., Sagebiel, E., Huebner, W., 2006. A preliminary analysis of seismological techniques to study Eros and other asteroids. Adv. Space Res. 37, 142–152.

Weissman, P., Asphaug, E., Lowry, S., 2004. Structure and density of cometary nuclei. In: Comets II. University of Arizona Press.

Yilmaz, O., 2001. Seismic Data Analysis,, Society of Exploration Geophysicists.